Misar and Otari
Future Journal of Pharmaceutical Sciences (2025) 11:115
https://doi.org/10.1186/s43094-025-00872-w

Future Journal of Pharmaceutical Sciences

RESEARCH Open Access

Molecular dynamics (MD) simulation-guided design and development of a cilostazol-CD-MOF inhaler and its in vitro evaluation in pulmonary fibrosis

Pranaya Misar[1,2*] and Kishor Otari[3]

Abstract

Objectives Cilostazol is a BCS class-II antiplatelet drug with a wide range of therapeutic actions, including anti-inflammatory, antioxidant, and antiapoptotic properties. Oral administration is associated with poor water solubility, limited absorption, and low bioavailability, which can be overcome by pulmonary administration. Despite of advancements, delivering poorly water-soluble drugs to the lungs with improved solubility, bioavailability, and stability and achieving excellent aerosolization continue to be substantial challenges.

Methods In this study, cilostazol was formulated as a dry powder inhaler using cyclodextrin metal–organic framework (CD-MOF), i.e., CLZ-CD-MOF by vapor diffusion method. Molecular docking and molecular dynamic simulation confirmed the formation of a cilostazol nanocluster with CD-MOF and its thermodynamic stability.

Results The free-energy estimation, hydrogen bond analysis, and the presence of CTAB confirmed the thermodynamic stability of cilostazol-CD-MOF with delta G of -6.4 ± 2 kcal/mol. Compared with CLZ-I formulation, i.e., micronized cilostazol with a DPI InhaLac®500, the cubic-shaped CLZ-CD-MOFs showed excellent aerodynamic performance owing to porous structure and lower density. The solubility of cilostazol significantly increased over a period of 24 h with the CLZ-CD-MOFs. The dissolution study showed that cilostazol was released more rapidly from CLZ-CD-MOFs than from the CLZ-I formulation, i.e., over 90% release within 15 min. The entrapment efficiency of CLZ-CD-MOF was approximately 96.39%. The CLZ-CD-MOF-F3 showed an EC50 value of 32.70 µg /ml in the A549 cell line, suggesting its potential in acute lung injury and pulmonary fibrosis.

Conclusion Therefore, γ-CD-MOF could be a safe and effective approach for delivering cilostazol to the lungs via dry powder inhalation.

Keywords MD simulation, Molecular docking, Cyclodextrin metallic organic framework, Cilostazol, Aerodynamic performance, Solubility, And dissolution

*Correspondence:
Pranaya Misar
misarpranaya@gmail.com
Full list of author information is available at the end of the article

Graphical abstract

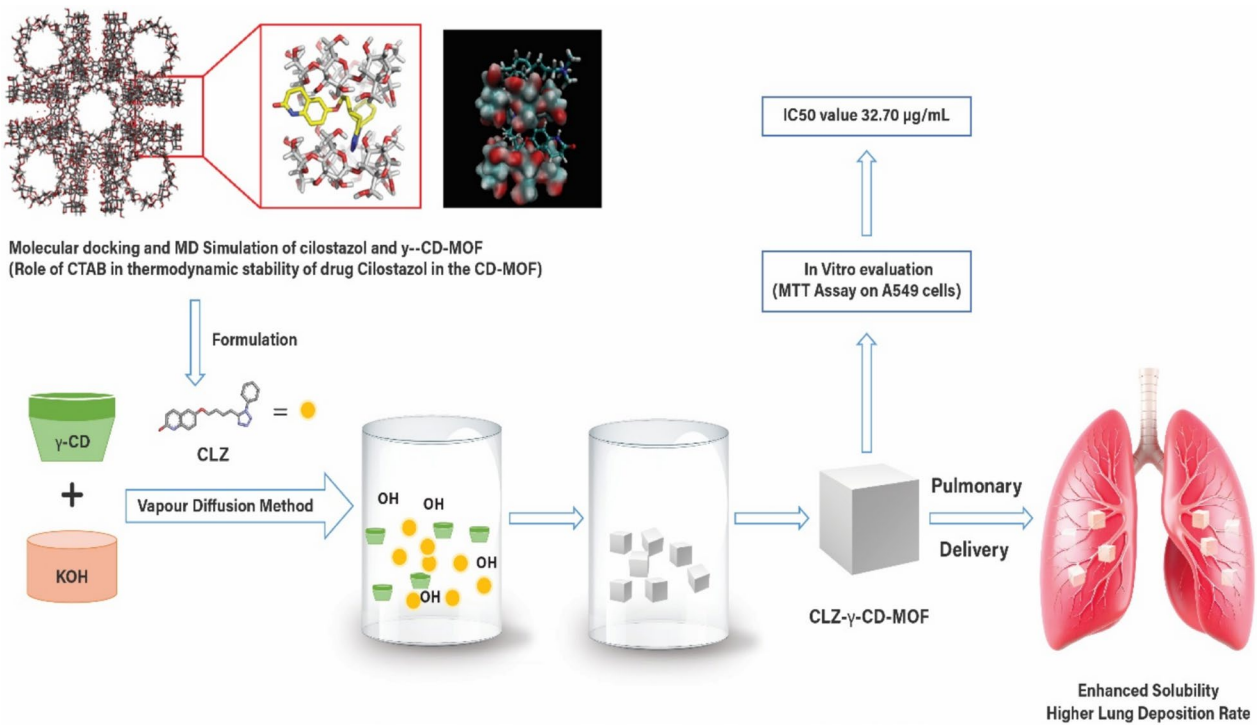

Background

The pulmonary route of drug administration, i.e., pulmonary drug delivery system, is a widely used effective approach to administer the drug directly to the lungs for local or systemic therapeutic effects [1, 2]. It is a targeted drug delivery system that delivers therapeutic molecules directly to the lungs with reduced doses and adverse effects for pulmonary diseases as well as improves the absorption of drugs in systemic diseases [3]. Systemic absorption of drugs occurs through the lungs due to its unique physiological characteristics, such as thin alveolar epithelium, large alveolar absorptive surface area with extensive capillary network, high perfusion, low chemical and enzymatic breakdown in the lungs, and short transfer path to systemic circulation [1, 2].The pulmonary drug delivery system (PDDS) possesses a series of benefits compared with other routes of administration, i.e., noninvasive route, rapid onset of action, improved bioavailability, prevention of g.i.t degradation, first-pass effect, more convenient, effective, and improved patient compliance [1–4].

The lungs natural defense mechanisms, i.e., macrophages phagocytosis and clearance function of the mucocilia act as a physiological barrier for pulmonary drug delivery. Despite of this, targeted pulmonary delivery of drug, inhalation remains a valuable approach as it offers rapid onset, devoid first pass, short path of absorption with minimum side effects [2, 4, 5]. Hence, inhalation could be used for treating acute lung injury, asthma, pulmonary fibrosis, chronic obstructive pulmonary diseases, bronchitis, respiratory infections, and lung cancer [2, 3].

The therapeutic effect of drugs in the lungs depends on the rate of lung deposition, which is directly related to the inhaled particle aerosolization performance. Aerosolization performance mostly depends on particle size distribution and structure [3]. Hence, for effective pulmonary drug delivery, aerosolization, lung deposition, and decreased macrophage phagocytosis and mucociliary clearance, particle engineering of size, shape, and surface morphology is required [4, 5]. Dry powder inhalers (DPIs) are a recent development in pulmonary inhalation therapy that have become more widely accepted than nebulizers and metered dose inhalers. Their popularity is attributed to several advantages, including convenience, cost-effectiveness, ease of use, good stability, and the fact that they do not contain a propellant [5, 6]. DPI uses the patients inspiratory force to deposit the drug deep in the lungs. Inhaled particles with an aerodynamic diameter

of 1–5 μm, a rough surface, and a non-spherical shape are more likely to have a higher rate of lung deposition. These particles are deposited in the trachea, bronchi, and alveoli with limited macrophage phagocytosis and mucociliary elimination [3–5].

Inhaled particles with an aerodynamic diameter of 1–5 μm, a rough surface, and a non-spherical shape are more likely to be deposited in the lungs. Once deposited, these particles are not easily cleared, as they have limited macrophage phagocytosis and mucociliary elimination [4, 5].

Despite recent developments in PDDS, improving the bioavailability of poorly water-soluble drugs for pulmonary administration continues to be challenging. The residence time and pharmacological effects of poorly water-soluble drugs in the lungs depend on their solubility and dissolution. The undissolved drug particles were eliminated from the lungs without exerting their pharmacological action due to mucociliary clearance in conducting zone and phagocytosis in the respiratory zone by alveolar macrophages. Insoluble particles have long residence times which may cause irritation and side effects [7–9]. Several strategies have been developed to increase the solubility and dissolution of insoluble drugs, such as amorphous solid dispersion [9], nanoparticles and cocrystals [9, 10], and micelles [11] but have limitations of poor thermodynamic stability, moisture adsorption, aerodynamic performance, and pulmonary toxicity, which affects the rate of lung deposition and bioavailability of drug [9–11].The nanocrystals hold a promising approach but tendency to aggregate alters its size, affects its deposition and bioavailability in lung [12, 13].

The novel technologies of porous particle were favorably employed to deliver the drug to the lung via dry powder inhaler due to its reduced density and small aerodynamic diameter to improve aerosolization performance [3, 14].The existing porous system with porogens has numerous limitations such as formation of in homogeneous and uncontrollable pores, risk of leakage of drug; and production of macropores with size greater than 50 nm, which results in fragmentation and friability of particles [3]. Hence, there is an urgent need to develop a nanoporous system without porogens to enhance the solubility and dissolution rate of water insoluble drugs with acceptable aerodynamic diameter and compatibility.

Metal–organic frameworks (MOFs) are newly developed crystalline porous drug materials commonly employed in drug delivery for the inclusion of significant pharmacological payloads because of their precise structure, high porosity, adjustable framework huge surface areas, relatively low toxicity, and easy chemical functionalization and diversity in terms of composition and functions. [15–17]. Cyclodextrin metal–organic frameworks (CD-MOFs) are MOFs having good compatibility and porosity, made up of cyclodextrin and potassium ions linked by the metal–ligand coordination bond to form the body-centered cubic extended structure having 7.8 A˚ aperture size and huge spherical pores with diameter 17 A˚ [16–18]. As per the previous research findings, the CD-MOFs are considered as a promising approach of pulmonary drug administration due to its i. cubic shape and nanoscale pores may provide excellent controllable aerosolization performance, ii. easy particle engineering may enhance lung deposition efficiency, iii. good biocompatibility due to its organic linker cyclodextrin which have proven safety and applicability for pulmonary delivery, and iv. single-step synthesis [3, 7, 18]. Drug molecules of appropriate size with carboxyl or hydroxyl functional groups can be easily inserted into the CD-MOF cavity via hydrogen bonding and electrostatic interactions. Furthermore, owing to its well-organized porous interior structure and large surface area, CD-MOFs act as versatile host to load enough amount of drug and convert crystal form of drug to molecular state; significantly enhancing the solubility and bioavailability of poorly water-soluble drug [19, 20] and used to deliver the number of drugs such as Fenbufen, Lansoprazole, Azilsartan, Ibuprofen, Ferulic acid, Diclofenac sodium, Curcumin, and Resveratrol [21]. It optimizes the bioavailability of drugs classified as BCS Class-II or IV by increasing their solubility rates and dissolution and solubilize drug by generating noncovalent complexes in solution by forming chemical complexes [22]. It demonstrated minimal cytotoxic effect against Calu-3 and A549 cells and did not alter physiology of lung or cause any inflammatory changes in lungs [23]. γ-cyclodextrin was preferred to prepared CD-MOF over other cyclodextrin owing to its larger cavity size (to encapsulate wide range of drug), higher water solubility (to improve dissolution and bioavailability), flexibility, and reduced toxicity [22].

Cilostazol, a BCS class-II antiplatelet drug with high permeability and low solubility, shows dissolution rate-dependent absorption, leading to suboptimal biopharmaceutical performance [24, 25]. It is clinically indicated for the treatment of ischemic diseases and claudication. It is a 2-oxyquinolones derivative, selective phosphodiesterase III, and adenosine uptake inhibitor that decreases the degradation of cAMP and elevates the cAMP concentration in the cell. PDE-III is broadly distributed in the heart, brain, blood vessels, liver, adipose tissue, and respiratory cells [26–28]. Hence, cilostazol affects multiple cells, including alveolar, platelet, adipose, myocyte, and smooth muscle cells [29]. In the lungs, increased intracellular cAMP is associated with anti-inflammatory, anti-fibrotic, vasodilatory, and antiproliferative effects. The competency of the lung and alveolar cell membranes

critically depends on cAMP regulation [26–28]. Cilostazol is widely used, affordable with a long usage history, and has various therapeutic actions, such as anti-inflammatory, antioxidant, and antiapoptotic actions [28, 30, 31]. Many researchers have designed and developed various cilostazol formulations to enhance its solubility, stability, and oral bioavailability of cilostazol but its oral administration is associated with the limitations such as significant first-pass metabolism, slower onset of action and risk of systemic adverse effect [28, 31]. The targeted pulmonary delivery overcomes these limitations of oral cilostazol. Hence, for the effective pulmonary delivery of cilostazol, it is necessary to improve its solubility, stability, and dissolution.

Therefore, MD simulation-guided dry powder inhaler (DPI) formulations of cilostazol–CD-MOFs were developed. Molecular modeling was carried out to confirm the formation of cilostazol nanoclusters with CD-MOF and to study the effect of CTAB on the thermodynamic stability of cilostazol in CD-MOF with free-energy estimation. In pulmonary drug delivery, the porosity and uniform three-dimensional architecture of CD-MOFs increase surface area, dispersity of particle and reduce its density, aids the transition of the crystal form of cilostazol into its molecular state, and facilitates aerosolization, absorption, and bioavailability. Vapor diffusion was used to prepare cilostazol-loaded CD-MOFs (CLZ-CD-MOFs). The aerodynamic performance, solubility, and dissolution rate of cilostazol were anticipated to be improved by the formulation. This research explores CD-MOFs as promising carriers for the pulmonary administration of poorly water-soluble drugs.

Methods

Material

Cilostazol was obtained from SDS Laboratories (Navi Mumbai). γ-cyclodextrin (γ-CD), methanol, potassium hydroxide (KOH), isopropanol, and cetyltrimethylammonium bromide (CTAB) were obtained from New Neeta chemicals (Chinchwad, Pune). InhaLac® 500 (Micronized Lactose Monohydrate) was purchased from Signet Excipients Pvt. Ltd. Mumbai. All chemicals procured were of analytical grade.

Molecular docking, MD simulations, and free-energy estimation

Modeling the system

In the present study, a system containing the complex of CD-MOF, i.e., cyclodextrin-based metal–organic framework with drug cilostazol and cetyltrimethylammonium bromide (CTAB), was initially generated. The Cambridge Structural Database (CSD) [32] with identifier LAJKUE [33] was used to obtain the crystal structure of CD-MOF. The crystallographic assembly of the CD-MOF downloaded from CSD has two primary types of caged enclosures: i) spherical voids, formed by six cyclodextrins (CDs), with a diameter of 1.7 nm, and ii) cavities, which occurs due to the face-to-face arrangement of the CD pairs, with a diameter of 0.8 nm. This type of cavity is referred to as a dual-CD cavity in this report. These caged enclosures can be visualized, as shown in Fig. 1.

Molecular docking

The system is generated in two stages. Initially, the complex of CD-MOF with cilostazol was generated using PyRx [34] that runs AutoDock 4.2 [35, 36] in the background, and in the second stage, the CTAB molecule was modeled in the system. In short, the CD-MOF was considered as a macromolecule, and cilostazol was docked as a ligand in the dual-CD cavity of CD-MOF as per the modeling procedure published by Zhou [37]. The grid center was set at the center of the dual-CD cavity with the default dimensions of the grid box to ensure the inclusion of the entire dual-CD cavity in pose prediction. The other docking parameters were set to default for the remainder of the procedure. The main objective of using

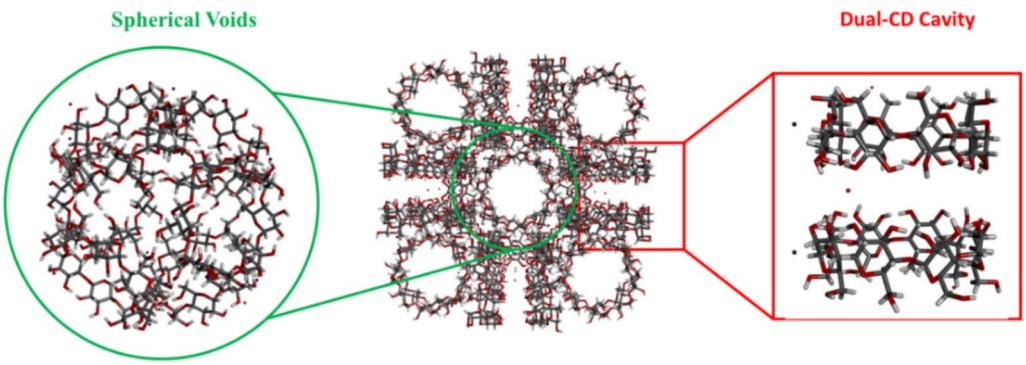

Fig. 1 Crystallographic assembly of the CD-MOF

AutoDock was to determine the initial geometry of the system. Moreover, the choice to select the dual-CD cavity of CD-MOF over spherical cages was made on the experimental finding that drug molecules like azilsartan and curcumin exhibited a preference for residing within the hydrophobic cavities of cyclodextrin (CD) pairs having a distance of 0.8 nm instead of occupying the larger spherical cavities of CD-MOF with a diameter of 1.7 nm [38, 39].

MD simulations

The poses of cilostazol and CTAB obtained from molecular docking were first cross-checked for the correctness of the bond order, and they were protonated and saved in mol2 format. The parameters and topologies of CD, cilostazol, and CTAB were obtained from the Swiss Param web server [40]. We conducted molecular dynamics (MD) simulations following a well-established protocol from our laboratory outlined in previous publications [41, 42] using NAMD [43]. Conventional molecular dynamics (CMD) simulations were performed using the CHARMM 22 force field [44, 45]. Briefly, the simulation protocol was initiated with the application of CMD conventions, subjecting the systems to 6000 energy minimization steps using the conjugate-gradient optimization algorithm. Subsequently, the temperature was gradually increased to over 300 ps simulation, incrementing by 0.001 at each integration step. Subsequently, an equilibration simulation was performed for 1 ns. Subsequent production runs with a time step of 2 ns, extended for 100 ns (ns).

Free-energy estimation

A widely recognized end point method, i.e., molecular mechanics Poisson–Boltzmann surface area (MMPBSA) approach was employed for free-energy estimation. The Café 1.0 plugin, which adeptly implements the MMPBSA method, was used for the calculations [46]. Operating as a powerful plugin, Café 1.0 utilizes TCL scripts integrated into VMD. To compute various energy terms in the free-energy calculations, NAMD and APBS [47] software were employed. The crucial structural data extracted from the final 100 frames of the trajectory were used for these free-energy calculations, ensuring that the system reached a general convergence state.

Preparation of cilostazol-loaded cyclodextrin metal–organic frameworks, i.e., CD-MOFs

CD-MOFs of cilostazol were formulated by the vapor diffusion method explained previously by Zhou et al. [7] 2020 for a poorly water-soluble drug. A γ-cyclodextrin and KOH with 32.40, 19.44 or 6.48 mg/ml and 11.20, 6.72 or 2.24 mg/ml, respectively, were mixed in 50 ml of deionized water and then filtered using filter of 0.8 µm. 10 mg/ml of cilostazol was dissolved in 35 ml of methanol using a sonicator. The obtained solution was then poured into the previously filtered solution with continuous stirring and incubated at 50^0C in a water bath. Thereafter, add 0, 40 or 80 ml of methanol and 2 mg/ml of CTAB to the solution with vigorous stirring. The obtained solution was kept for 2 h at room temperature, centrifuged to obtain the CLZ-CD-MOFs, and repeatedly washed with isopropanol. Moreover, during washing, the CLZ-CD-MOFs were neutralized with acetic acid and at the end were vacuum dried for 24 h. Table1 illustrates the formulation details.

In this study, the widely employed DPI InhaLac®500 was used as a commercial carrier for the preparation of cilostazol inhalation formulation; cilostazol was micronized using a jet mill and then mixed with InhaLac®500 and used for comparative study.

Characterization

Particle morphology

Morphological characterization, i.e., shape of particles of all samples was observed by scanning electron microscopy (FEI Quanta 200, Netherland, xT Microscope software, Source; Tungsten Filament) with a working distance of 10 mm, spot size of 3 mm, and 15.0 kV accelerating voltage. Prior to microscopy, the samples were immobilized on a metal stub using a two-way adhesive strip and then sputter coated with gold under vacuum. Images were acquired using the xT Microscope.

Particle size distribution

Particle size was analyzed with Zetasizer Nano ZS90 (Malvern Instruments), Malvern at 25 °C by photon correlation spectroscopy. Prior to the measurement diluted the samples with deionized water. Particle size was analyzed using Malvern Instruments' dispersion technology software. The polydispersity index (PDI), i.e., dimensionless number predicting the width of the size distribution, was also computed.

Table 1 Formulation details of CLZ-CD-MOF F1, CLZ-CD-MOF F2, and CLZ-CD-MOF F3

Materials (quantity)	F1	F2	F3
γ-CD (mg /ml)	32.40	19.44	6.48
KOH (mg /ml)	11.20	6.72	2.24
Cetyltrimethylammonium bromide (CTAB) (mg /ml)	2	2	2
Methanol (ml)	0	40	80

Crystallinity

X-ray powder diffraction (XRPD) was used to assess the crystallinity of the formulation. XRD of the pure drug and CLZ-CD-MOFs was analyzed using BRUKER AXS D8 advance Karlsruhe, Germany, from RCPIPER (Shirpur, India). Samples were prepared using glass plate in which the sample was spread and detected at 2Θ range of 5–60° at 35 mA and 40 kV by scanning at a resolution step length of 0.02°.

Differential scanning colorimetry (DSC)

DSC was used to assess the thermal stability and compatibility of drug and excipients. Thermal behavior of the drug was studied using differential scanning calorimeter (METTLER DSC 30 S, Mettler Toledo, Switzerland). The small quantity of sample was crimped between the aluminum pans using hydraulic press. The pans were heated at the rate of 5 °C /min from 30 to 250 °C in the presence of 50 ml /min nitrogen gas.

Attenuated total reflectance-fourier transform infrared (ATR-FTIR)

ATR-FTIR (Bruker Optik GmbH, Ettlingen, Germany) is used to analyze samples directly; preparing the samples by using KBr is not necessary. If the material is two-sided, it will be essential to conduct the analysis on both sides as the analysis is shallow and the depth corresponding to the spectral region covered is less than 4 μm. The quality of the spectrum is dependent on proximity between the sample and the diamond crystal. A high-pressure regions clamp is used to attain this result. Chemical identification of CLZ in solid state was accomplished using ATR-FTIR analytical characterization as well as compatibility study with excipients γ-cyclodextrin and CTAB. Initially, the diamond ATR crystal had been wiped with isopropanol, a cleanness test function was run, and a fresh background measurement was taken before sample analysis. Then, clamp was used to apply the pressure to solid sample to compress it against ATR crystal. Then, spectrum was captured in the 4000 to 400 cm^{-1} spectral regions.

Surface area and pore diameter

BET, i.e., Brunauer–Emmett–Teller (Quantachrome St 2 on NOVA touch 4LX) analysis is an important analytical method to determine the surface area and pore diameter of samples by adsorption–desorption of nitrogen. Prior to the analysis outgassed all the samples for 6 h at 50 °C.

Bulk and tapped densities

A graduated glass cylinder was used to calculate the bulk and tapped densities of the samples. The samples were poured into an empty graduated glass cylinder, and the initial volume was recorded as the bulk volume. Then, the cylinder was tapped until the volume of samples remained constant, and the final volume was recorded as the tapped volume. The bulk and tapped densities were calculated using the ratio of the mass of the samples divided by the corresponding bulk and tapped volumes.

Angle of repose

The angle of repose was determined by fixed funnel method. The funnel was fixed to the iron stand placed on the table surface at approximately 3.0 cm from the bottom of the table. The samples were poured through the funnel, and the formation of a cone on the surface was observed. The angle of the cone was recorded as the angle of repose.

Entrapment efficiency

Entrapment efficiency was used to calculate the percentage of drug entrapped in the formulation compared with the total amount of drugs utilized for the formulation. In a 100-ml flask, dissolve dry powder equivalent to 10 mg cilostazol in methanol. Dissolve 2 ml of the obtained solution into in 100-ml measuring flask. The UV–vis spectrophotometer (UV-1800 Shimadzu, Japan) was used to record absorbance at a maximum wavelength of 257 nm. The cilostazol concentration was determined using a linear regression equation. % EE, i.e., the percentage entrapment efficiency can be calculated using the following formula:

$$\text{EE (\%)} = (\text{Actual concentration of cilostazol used}) / (\text{Determined concentration of cilostazol}) \times 100$$

Aerodynamic performance analysis

The aerodynamic particle size distribution for all inhaled drugs is a crucial measure that directly influences regional deposition in the respiratory tract, as well as the lungs. The aerodynamic performance of the formulations was evaluated using the Anderson cascade impactor (Tokyo Dyrec AN200). The Anderson cascade impactor sampler consists of inlet nozzles and eight impactor stages to modify the drug flow. Each stage consisted of nozzle plates with multiple nozzles to direct the airflow to the filter-coated removable impaction plates positioned below each stage of the nozzles to collect the impacted particles. The remaining particles were collected using a final inertial filter or collector. The distance between the nozzle exits and the filter surface was 48 mm to ensure uniform collection of particles on the backup filter positioned next to the inertial filter. The sampler was designed to operate at 28.3 L /min. The inertial

filter consists of a plastic holder with a length of 9 mm and a diameter of 4 mm, in which the webbed stainless steel filters are supported by the crossed 200 µm stainless steel wires. The administered dose was 20-mg powder**.** The product strengths were F1-0.012 mc, F2-0.020 mc, F3-0.076 mc, and Inhale- 0.08 mc**.** The inertial filter was designed such that the webbed stainless steel filters were packed on the support of crossed 200 µm stainless steel wires in a plastic holder with a diameter of 4 mm and length of 9 mm. The mean mass aerodynamic diameter (MMAD), fine particle fraction (FPF), and other aerodynamic performance parameters were evaluated by software Inhalytix 5000 (32bits, Copley Scientific, Nottingham, UK) with a 60 L/min flow rate for 4 s and repeated four times.

Saturation solubility and dissolution studies

The cilostazol and CLZ-CD-MOF were evaluated for their saturation solubility, samples containing 2 mg equivalent of cilostazol were dissolved into 30 ml of solution of phosphate buffer (PBS, pH 7.4), and the release medium was incubated in an air bath (37.0 °C) with 100-rpm shaking speed. After centrifugation, 1 ml of supernatant was collected at predetermined time intervals and another 1 ml of freshly prepared PBS was poured again to compensate for the loss of solution during sampling. UV spectroscopy was used to analyze the obtained samples. Dissolution studies of formulations were conducted under sink conditions with a 100-rpm shaking speed in an air bath at 37.0 °C. The samples of equivalent quantities of cilostazol were dissolved in 7 ml of PBS containing 1% SD, i.e., sodium dodecyl sulfate. After centrifugation at 5000 rpm, supernatants were collected at predetermined time intervals and compensated with an equivalent volume of fresh dissolution fluid. UV spectroscopy was used to determine the cilostazol concentration in the dissolution fluid.

Cytotoxicity study (MTT assay)

The MTT assay used A549 cells derived from lung carcinoma [48], specifically human alveolar adenocarcinoma, for the cell toxicity study. The cells were cultured for 3 h at 37 °C, at a density of 1 million cells per milliliters with 6.5% CO_2 and 75% relative humidity. Cells were placed in a culture medium at a density of 50,000 cells/well, and various amounts of compounds were added to the microplates. The cultures were incubated at 37 °C and 6.5% CO_2 for 24 h. After that, 20 µl of the MTT labeling mixture was added, and the combination was incubated for 24 h at 37 °C, 6.5% CO_2, and 75% relative humidity.100 µL of DMSO solubilization solution was added to each well and incubated overnight. A microplate ELISA reader was used to measure the absorbance of samples. Based on the filter options in the ELISA reader, the optimal wavelength range, i.e., between 540 and 600 nm, was selected to measure the formazan product's absorbance. The cytotoxicity study data were examined by measuring the absorbance and corresponding chemical concentrations.

The following formula was used to calculate the cytotoxicity percentage or cell growth inhibition percentage:

$$\% \text{ Cytotoxicity} = (A - \text{control} - A - \text{test})/[A - \text{control}] \times 100\%$$

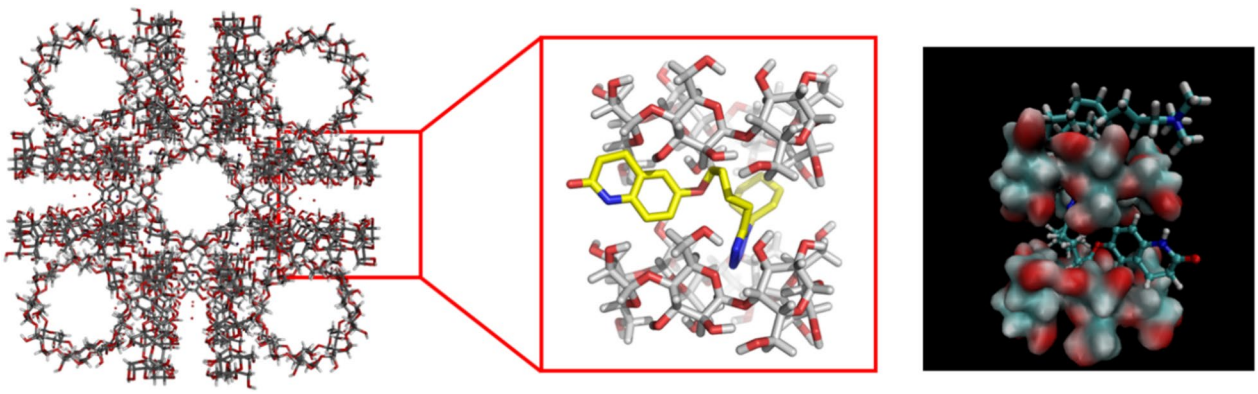

Fig. 2 Crystallographic CD-MOF (left) and the results of docking drug cilostazol (yellow sticks) in the dual-CD cavity (white sticks) as shown in the white background. The entire system with CD-MOF (surface representation), cilostazol (ball and stick representation), and CTAB (stick representation) are shown in black background

The IC50 value of CLZ-CD-MOF-F3 in A549 cells was determined using GraphPad Prism10 (GraphPad Software, Inc., San Diego, USA).

Results and discussion

Molecular docking and MD simulation

Molecular docking

The results obtained from molecular docking can be visualized as shown in Fig. 2. Cilostazol was found to be stabilized by numerous noncovalent interactions like hydrophobic interactions, hydrogen bonds, and van Der Waal's contacts. The use of MD simulations to estimate free energy offers several advantages over molecular docking methods. MD simulations provide a dynamic representation of molecular interactions, enabling the exploration of conformational changes and flexibility in ligand-receptor binding. Unlike molecular docking, MD simulations capture the temporal evolution of a system, enabling a more realistic depiction of the binding events involved. This dynamic perspective is particularly valuable for systems with flexible and dynamic bindings. These facts provide a more accurate representation of the thermodynamics of the binding process and enhance the realism of the environment, contributing to the precision of free-energy calculations. Overall, MD simulations offer a robust and comprehensive approach for free-energy estimation, considering the dynamic nature of molecular interactions and providing insights that may be overlooked in static molecular docking studies. Therefore, the objective of performing molecular docking here was to obtain the initial confirmation of the CD-MOF with cilostazol and CTAB. The detailed interaction analysis and free-energy estimation data were derived from subsequent MD simulations.

MD simulations

Table 2 summarizes the free-energy calculation results for systems with and without CTAB. The systems with CTAB exhibit a delta G of -6.4 ± 2 kcal/mol, with notable contributions from favorable van der Waals interactions (-30.5 ± 2 kcal/mol) and polar solvation (30.2 ± 3 kcal/mol). The electrostatic contribution (delta Ele) is -6.1 ± 2 kcal/mol, indicating a favorable interaction. In contrast, the systems without CTAB display a slightly higher delta G of -3.9 ± 2 kcal/mol, with decreased contributions from van der Waals interactions (-26.2 ± 2 kcal/mol) and polar solvation (26.4 ± 3 kcal/mol). The electrostatic contribution (delta Ele) is -8.7 ± 2 kcal/mol, indicating a less favorable interaction. These findings elucidate the effect of CTAB on the energetics of the studied systems, emphasizing the role of specific interactions in the modulation of free-energy changes. The free-energy difference between the two systems clearly indicates a significant role of CTAB in defining the thermodynamic stability of cilostazol in the CD-MOF.

During MD simulations, hydrogen bonding interactions between CD-MOF and the ligand were investigated, and the occupancy of these interactions was traced and discussed in Table 3. Hydrogen bond donors and acceptors involved in the interactions were identified, with CD-MOF frequently acting as a hydrogen bond acceptor from the ligand. The occupancy values recorded for these interactions during the simulation were noteworthy, at 38.90, 1.10, and 0.70%. Additionally, the ligand displayed hydrogen bonding interactions with CD-MOF as a donor, with occupancy values of 2.80, 12.60, and 0.70%. These occupancies correspond to the hydrogen bonds formed between the three free hydroxyl groups from the CD-MOF. These results provide insights into the dynamic nature of the hydrogen bond between the ligand and CD-MOF, emphasizing the varying degrees of occupancy for specific donor–acceptor pairs throughout the simulation.

Hydrogen bonding analysis

Evaluation of synthesis and particle characteristics of cilostazol-CD-MOFs

CLZ-CD-MOFs were formulated using the vapor diffusion method. A series of CLZ-CD-MOFs were prepared as per the procedure, indicated as CLZ-CD-MOF-F1, CLZ-CD-MOF- F2, CLZ-CD-MOF- F3, and CLZ-I, to investigate the properties of the particles and the influence of different manufacturing conditions on the particle characteristics.

The desired particle size, i.e., 1–5 µm and the cubic morphology of all three formulations and CLZ-Inhalac were observed from the SEM images. All three CLZ-CD-MOFs were cubic in shape; however, but; CLZ-CD-MOF-F3 had a larger particle size (Fig. 3). On the other hand,

Table 2 Free-energy calculations of the systems with and without CTAB

System	Δ Ele	Δ Vdw	Δ PB	Δ SA	Δ Gas phase	ΔSolvation	Δ Polar	Δ Nonpolar	Total Free Energy ΔG
With CTAB	-6.1 ± 2	30.5 ± 2	34.8 ± 3	-4.6 ± 0.1	-36.6 ± 3	30.2 ± 3	28.7 ± 2	-35.1 ± 2	-6.4 ± 2
Without CTAB	-8.7 ± 2	-26.2 ± 2	35.2 ± 4	-4.1 ± 0.2	-35 ± 4	31 ± 4	26.4 ± 3	-30.3 ± 2	-3.9 ± 2

Table 3 Summary of the six hydrogen bonds traced in the simulation between various functional groups from cilostazol and the CD-MOF

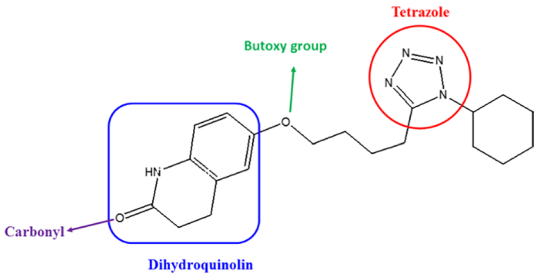

Donor	Acceptor	Occupancy
CD-MOF	Lig (Tetrazole)	38.90%
CD-MOF	Lig (Carbonyl)	1.10%
CD-MOF	II (butoxy group)	0.70%
Lig (NH from dihydroquinolin group)	CD-MOF (Hydroxyl group 1)	2.80
Lig (NH from dihydroquinolin group)	CD-MOF (Hydroxyl group 2)	12.60
Lig (NH from dihydroquinolin group)	CD-MOF (Hydroxyl group 3)	0.70

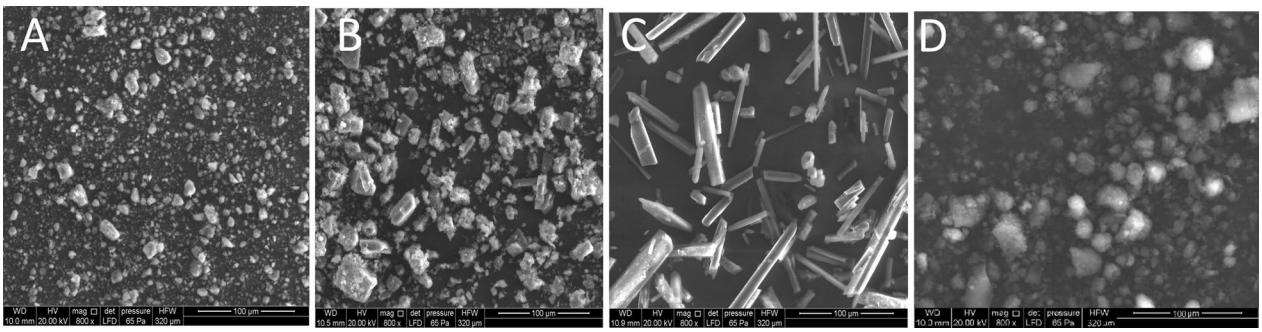

Fig. 3 SEM, i.e., scanning electron microscopy images of cilostazol-CD-MOFs. a. CLZ-CD-MOFs -F1 b. CLZ-CD-MOFs -F2 c. CLZ-CD-MOFs-F3 d. Cilostazol-inhalac

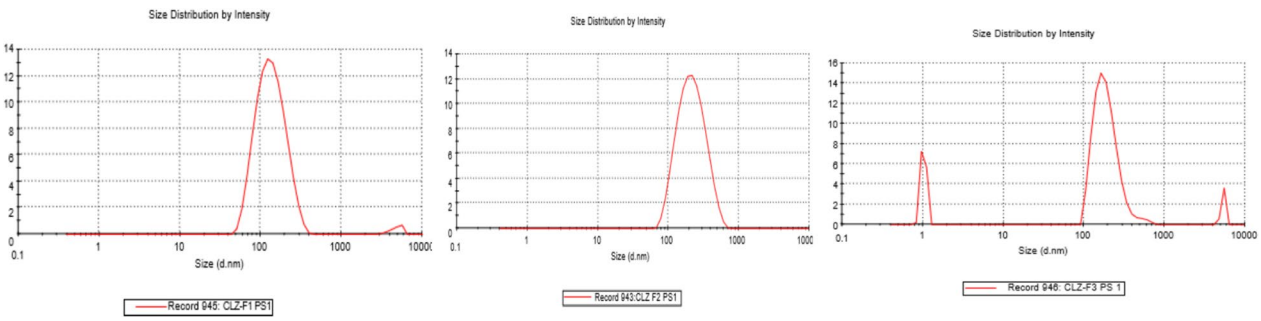

Fig. 4 Particle size distribution of the CLZ-CD-MOFs by intensity. CLZ-CD-MOF-F1, CLZ-CD-MOF-F2, and CLZ-CD-MOF-F3

owing to the lower concentration of γ-CD and KOH, crystals of CLZ-CD-MOFs were not formed. Photon-correlation spectroscopy was used to study the particle size distribution of the CLZ-CD-MOFs. A Zetasizer Nano ZS90 instrument was used to assess the median particle size and intensity at 25 °C (Fig. 4) CLZ-CD-MOF-F1,

CLZ-CD-MOF-F2, and CLZ-CD-MOF-F3 had average median particle sizes of 117.6, 191.6 and 248.7 nm, respectively. The CLZ-CD-MOF-F3 shows three peaks having percent intensity 82.7, 13.1 and 4.2%. The particle size of the formulation inversely depends on the volume of methanol, i.e., the particle size of CLZ-CD-MOFs increases with decreasing methanol volume. According to the research findings, there are two basic steps in the development process of MOFs, i.e., nucleation, and crystal growth [48]. At the initial stage, small crystals of dissolved precursors in solution were precipitated, which acted as the nucleus center of crystallization. In the next crystal formation stage, the formation units adhered to the preexisting nuclei, eventually organizing themselves as a crystalline structure.

Due to γ-CD's poor solubility in methanol, the addition of methanol causes γ-CD to become more supersaturated, resulting in faster nucleation and production of a high degree of supersaturation, which in turn enhances the nucleation rate and the formation of many nuclei. As a result, the smallest nuclei initially precipitated, which led to a final decrease in CLZ-CD-MOF particle size. Particle size was not significantly affected by changes in γ-CD and KOH concentrations (Fig. 3a and c). The results showed that the percent distribution of particles based on intensity and polydispersity index (PDI) for all the formulations was found to be in the range of 84.5–100% and 0.19–0.53, respectively. PdI is a dimensionless quantity with a range of 0 to 1 and, is used to characterize the particle size population distribution. A PdI value greater than 0.7 indicates a broad range of particle size distributions [49]. All CLZ-CD-MOFs had median particle sizes varying from 0.5 to 5 µm, which is the ideal aerodynamic particle size for delivering drugs to the lungs.

The X-ray diffraction patterns of cilostazol and CLZ-CD-MOFs are shown in Fig. 5a the powder X-ray diffraction pattern of pure cilostazol matched with those previously reported and revealed significant intense peaks at 12.67, 12.98, 15.35, 15.76, 17.98, 18.71, 19.52, 22.19, and 22.58 degrees [50, 51]. After CLZ loading into γ-CD-MOF, the intrinsic peaks of CLZ crystals disappeared, attributed to cilostazol entrapment in the nanopores of γ-CD-MOF in its molecular state. The results were supported by the data of DSC illustrated in Fig. 5b which shows that the melting point of cilostazol was 160.75°C, like those reported in literature and the intense peaks of the cilostazol disappeared which indicate the successful loading of cilostazol in CD-MOFs with melting point 159.80°C.

The drug loaded was 10 µg/ml of solution; accordingly, the entrapment efficiency of the formulations was calculated, i.e., CLZ-CD-MOF-F1, CLZ-CD-MOF-F2, and CLZ-CD-MOF-F3 were found to be 87.01, 94.54, and 96.39%, respectively, based on the linear regression equation $y = 0.0651x + 0.0035$ with $R^2 = 0.9986$ with the practical yield 8.701, 9.454, and 9.6390, respectively. [52] as illustrated in Fig. 6b.

In the drug-excipient compatibility study, in IR spectrum of cilostazol (Fig. 7), peak occurred at 1663 cm^{-1} represented aryl ketone group. The other chemical groups present are discussed in Table 4 and confirmed the presence of -NH group, i.e., secondary amine, -CH stretching, i.e., aromatic ring, -CH2- group, i.e., aliphatic chain, and -C=C bending. The FTIR spectra of pure cilostazol and physical mixture, i.e., CLZ-γ-cyclodextrin

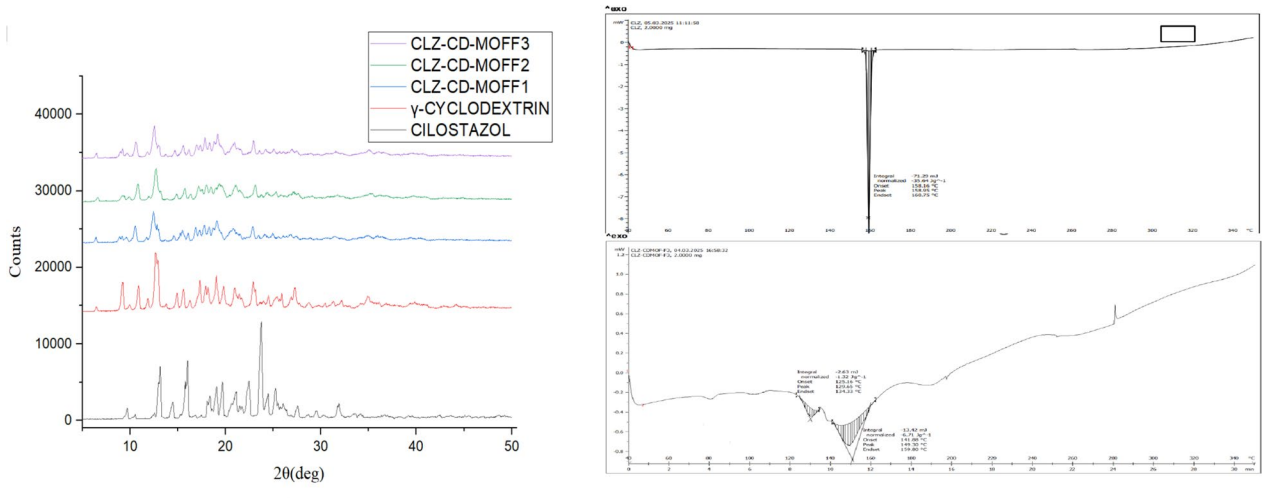

Fig. 5 **a** X-ray diffraction patterns of cilostazol and CLZ-CD-MOFs. **b**1. DSC of cilostazol and 2. CLZ-CD-MOF-F3

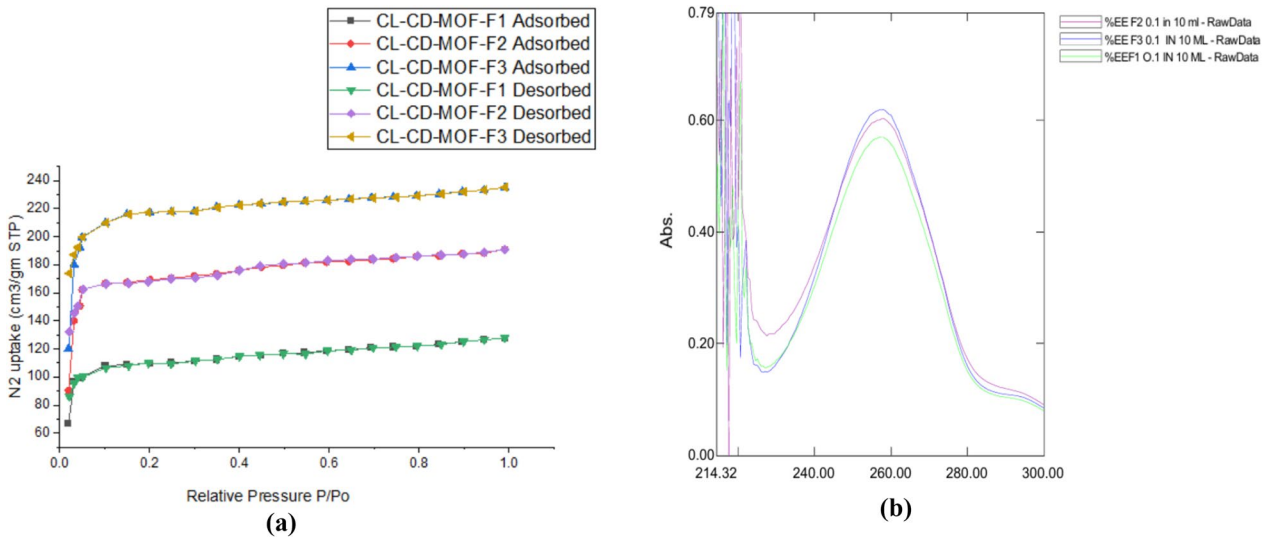

Fig. 6 **a** N_2 uptake, adsorption, and desorption isotherms of CLZ-CD-MOFs. **b** Spectrum overlay of entrapment efficiency of all CLZ-CD-MOFs

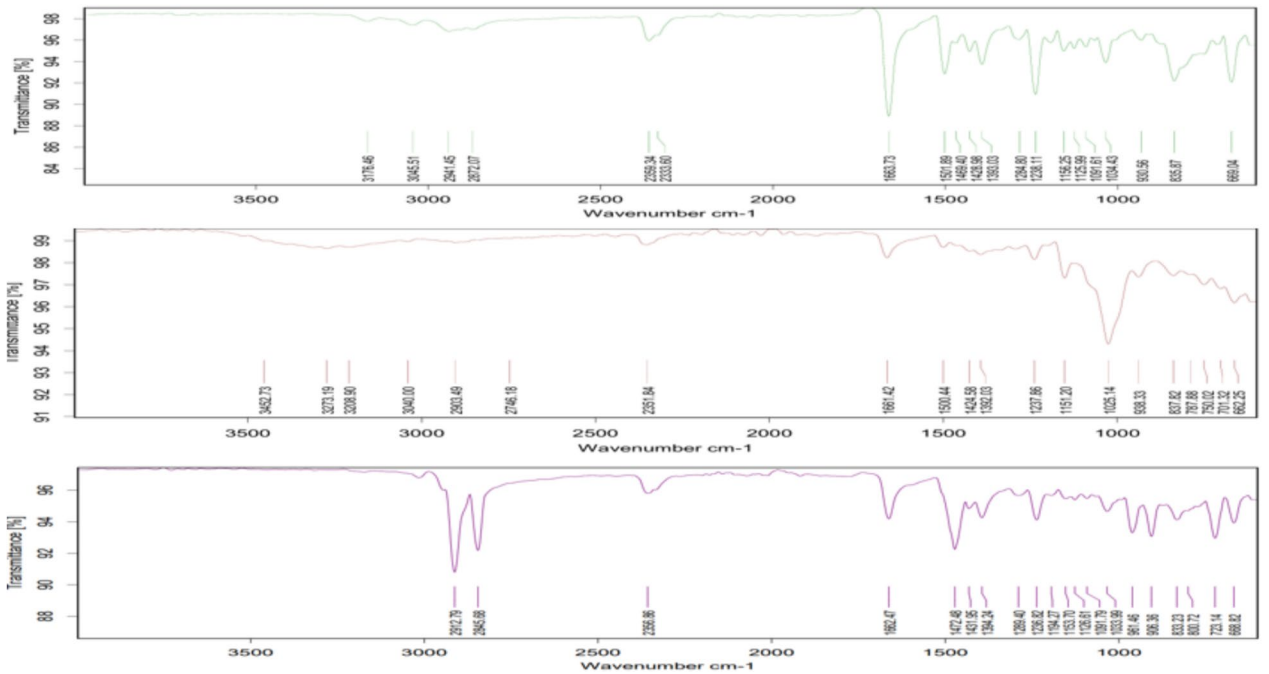

Fig. 7 FTIR spectrum of **a** Cilostazol, **b** Physical mixture of CLZ-γ cyclodextrin, **c** Physical mixture of CLZ-CTAB

and CLZ-CTAB, were compared. All the peaks present in the FTIR spectrum of cilostazol were present within the standard rages of functional groups of physical mixture. The obtained FTIR does not shown any significant peak shifting. So, it can be concluded that there were no significant variations in the major peaks of both the spectra indicating that the drug and excipient are compatible with each other and are non-interacting (Table 5).

The angle of repose provides information about the adhesion and flow characteristics of powders [53]. A lower angle of repose indicates improved powder flowability. Table 6 illustrates that all the formulations show a similar angle of repose as that of the CLZ inhalation formulation. Owing to the porous structure of CD-MOFs, tapped density and bulk density of CLZ-CD-MOFs were lower than those of the CLZ inhalation formulation. BET analysis was used to measure the surface area and pore

Table 4 IR spectra of cilostazol: Functional groups, standard peaks, and observed peaks present in FTIR spectrum cilostazol

Functional group	Standard range (cm^{-1})	Observed peaks (cm^{-1}))
-NH (Secondary Amine)	3500–3200	3176
-CH Stretching (Aromatic)	3100–3000	3045
-CH2 Stretching aliphatic	3000–2850	2941
-CH2 Stretching aliphatic	3000–2850	2872
-C = O Stretching aryl ketone	1680–1660	1663
-C = C bending	1500–1450	1501
-C = C bending	1500–1450	1469
-C–O–C- stretching	1300–1000	1238

Table 5 Surface area, pore volume, and pore diameter of CLZ-CD-MOF-F1, CLZ-CD-MOF-F2, and CLZ-CD-MOF-F3

Sample Name	Surface Area (m^2/g)	Pore diameter(nm)	Pore Volume (cm^3/g)
y-CD-MOF	790	1.86	0.567
CLZ-CD-MOF-F1	12	0.3641	0.231
CLZ-CD-MOF-F2	7.08	0.3362	0.193
CLZ-CD-MOF-F3	6.06	0.3063	0.129

Table 6 Angle of response, bulk density, and tapped density of CLZ-CD-MOF-F1, CLZ-CD-MOF-F2, CLZ-CD-MOF-F3, and CLZ-I (mean ± S.D., n = 3)

Sample	Angle of repose (°)	Bulk density (mg/cm^3)	Tapped density (mg/cm^3)
F1	46.36 ± 0.60	79.46 ± 1.45	100.33 ± 2.30
F2	45.5 ± 1.73	80.73 ± 1.62	180.23 ± 1.80
F3	45.0 ± 1.04	82.03 ± 1.25	104.40 ± 3.01
CLZ-I	43.36 ± 1.22	119.46 ± 1.45	191.16 ± 1.05

diameter of CLZ-CD-MOFs by the nitrogen adsorption–desorption isotherms (Fig. 6a). Table 5 shows that according to the BET single-point method, the BET surface area of γ-CD-MOF was found to be 790 m^2/g. The loading of cilostazol into the γ-CD-MOF showed a large reduction in surface area as cilostazol occupied the pores of the crystal and hindered the nitrogen uptake. The BET surface areas of CLZ-CD-MOF-F1, CLZ-CD-MOF-F2, and CLZ-CD-MOF-F3 were 12 m^2/g, 7.08 m^2/g, and 6.06 m^2/g, respectively. There was a correlation between the surface area and particle size; as the surface area decreased, and the particle size increased. According to the BJH pore size distribution-desorption method, summarized in Table 5, the pore diameter of γ-CD-MOF was found to be 18.6 Å and pore diameter of CLZ-CD-MOF-F1, CLZ-CD-MOF-F2, and CLZ-CD-MOF-F3 was approximately 3Å and confirmed the porous nature of CLZ-CD-MOFs; the encapsulation of cilostazol showed a large reduction in pore diameter and pore volume, i.e., porosity.

Aerodynamic diameter

Dry powder inhalation achieves pharmacological effects via dispersion, atomization, deposition, and then absorbed by the lung tissues and blood vessels. Thus, the deposition of the particles was the key factor for CLZ-CD-MOF formulation to achieve efficient lung deposition. To investigate the dispersibility and aerodynamic properties of the CLZ-CD-MOF dry powders, the aerosol performance of the powders was characterized by the Anderson cascade impactor. The aerodynamic performance of the formulations was evaluated further. The FPF value is the percentage of all particles that have an aerodynamic diameter of less than 5 μm, and it is frequently used to forecast the quantities of particles eventually deposited in the lungs after pulmonary delivery of the drug. CLZ-CD-MOF-F1, CLZ-CD-MOF-F2, and CLZ-CD-MOF-F3 showed much greater FPF values than that of the cilostazol inhalation formulation, revealing the better aerodynamic performance of CLZ-CD-MOFs as shown in Fig. 8a and d. Density is a crucial component of DPI formulations that significantly affects aerosolization behavior. The porous structure of CD-MOF was frequently used to improve the aerodynamic behavior for pulmonary delivery of drugs as they may significantly lower the microparticle density [53, 54]. Drugs with low-density particles are more effectively delivered to the lungs due to their increased dispersibility and lung deposition [53, 54]. As shown in the Table 6, CLZ-CD-MOFs formulations were much less dense (i.e., possesses lower density) than nonporous cilostazol inhalation formulations. The mean aerodynamic diameter of the particles is represented by the MMAD. Figure 8c represents that all formulations had no significant differences in their MMAD values. Figure 8b shows that all CLZ-CD-MOF formulations had larger emitted dose values than that of the cilostazol inhalation formulation, demonstrating that CLZ-CD-MOFs were well dispersed.

Saturation solubility and dissolution

The solubility and dissolution rate of inhalation formulations of poorly water-soluble drugs affect their bioavailability in the lungs. After pulmonary deposition, dissolution competes with two main mechanisms for lung clearance: transport via the mucociliary escalator and macrophage uptake. Figure 9 represents the saturation

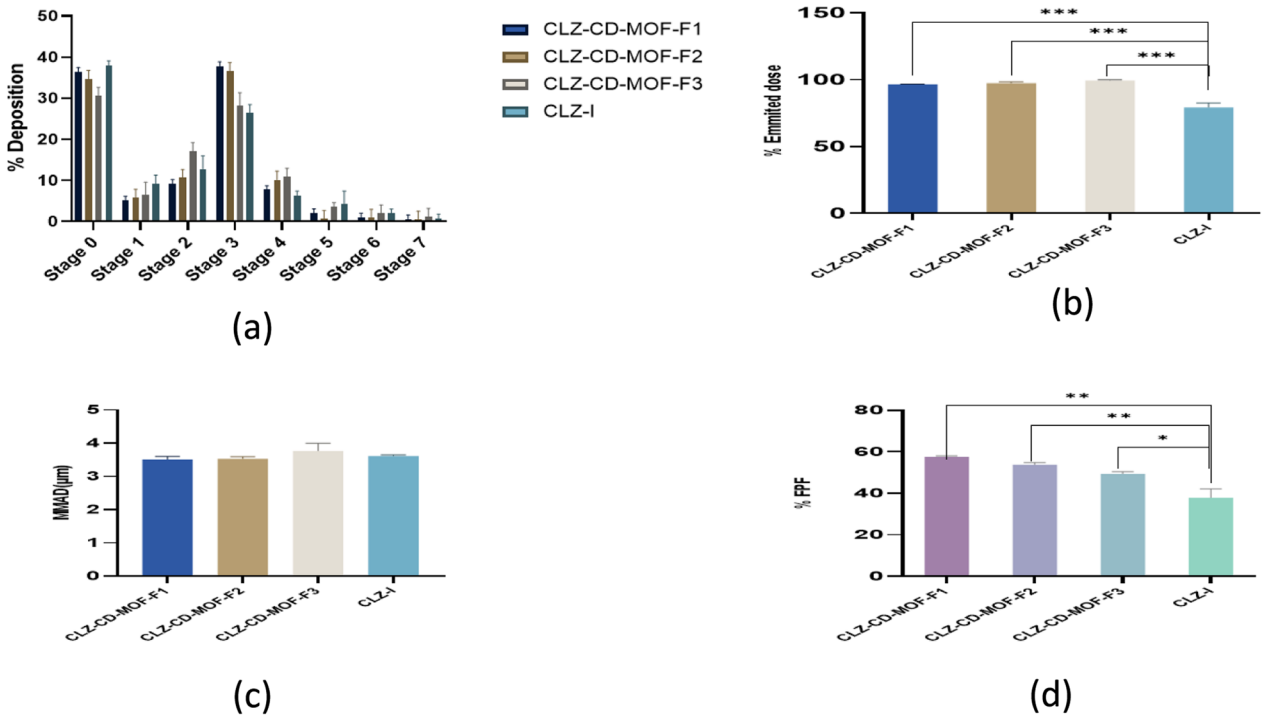

Fig. 8 **a** Percentage drug deposition of CLZ-CD-MOF-F1, CLZ-CD-MOF-F2, CLZ-CD-MOF-F3, and CLZ-I using Anderson cascade impactor at 60 L/min (mean ± S.D., $n = 3$). **b** MMAD, i.e., mass median aerodynamic diameters of CLZ-CD-MOF-F1, CLZ-CD-MOF-F2, CLZ-CD-MOF-F3, and CLZ-I (mean ± S.D., $n = 3$). **c** % Emitted dose of CLZ-CD-MOF-F1, CLZ-CD-MOF-F2, CLZ-CD-MOF-F3, and CLZ-I (mean ± S.D., $n = 3$). **d** % FPF value of CLZ-CD-MOF-F1, CLZ-CD-MOF-F2, CLZ-CD-MOF-F3, and CLZ-I (mean ± S.D., $n = 3$). Significant difference is regarded as $p < 0.05$, * implies $p \leq 0.05$, ** implies $p \leq 0.01$, *** implies $p \leq 0.001$

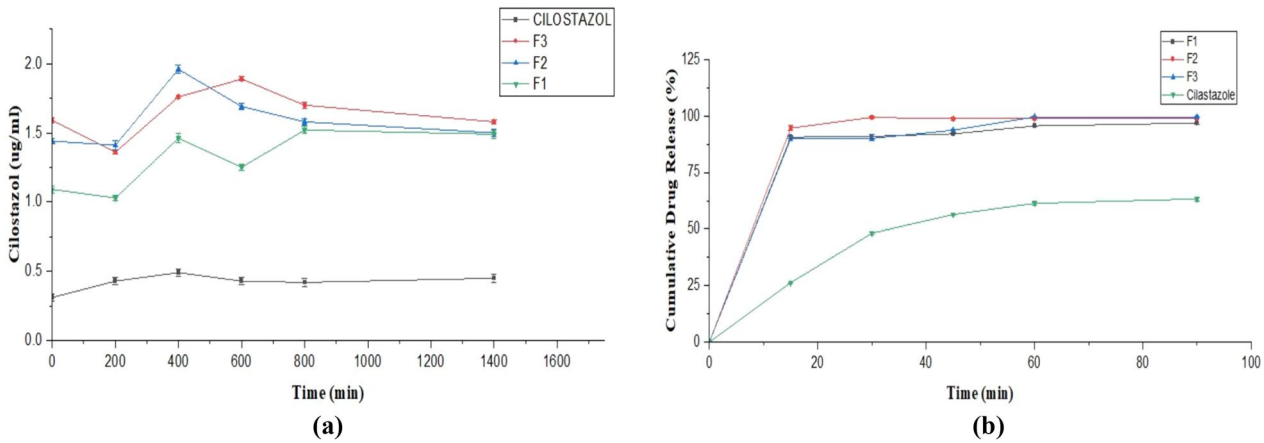

Fig. 9 **a** Saturation solubility of CLZ-CD-MOF-F1, CLZ-CD-MOF-F2, and CLZ-CD-MOF-F3 at 37 °C (mean ± S.D., $n = 3$). **b** In vitro dissolution studies of CLZ-CD-MOF-F1, CLZ-CD-MOF-F2, and CLZ-CD-MOF-F3 under sink condition (mean ± S.D., $n = 3$)

solubility and dissolution profiles of the formulations. γ-CD and MOF are a hybrid system, create a highly porous matrix with increased surface area and adjustable pore sizes, allowing controlled cilostazol loading and release by regulating diffusion, dissociation, and degradation. Specifically, cilostazol release from the MOF is primarily governed by diffusion, with the rate determined by the MOF's pore dimensions, porosity, surface area, and the concentration gradient. Subsequently, as the surrounding environment dilutes, cilostazol detaches from the cyclodextrin cavity. Finally, the MOF structure itself may degrade, contributing to the complete release of the

drug by diffusion. As presented in Fig. 9a, there was a considerable improvement in the solubility of cilostazol, CLZ-CD-MOF-F1, CLZ-CD-MOF-F2, and CLZ-CD-MOF-F3 over a 24 h period. The solubility values for cilostazol, F1, F2, and F3 were 0.45, 1.53, 1.65, and 2.1 µg/ml, respectively, indicating that CD-MOFs increased the solubility of cilostazol. As per previous research findings, the volume of alveolar fluid in the lung is only approximately 36 ml, and alveolar surfactant improve the dissolution rate of drugs [53, 54]. Hence, it is important to conduct dissolution under sink conditions. To minimize the influence of particle size on dissolution, CLZ-I was selected for comparison as it contained micronized CLZ. As illustrated in Fig. 9b, the rate of dissolution of CLZ-CD-MOFs was impressively higher, and within 15 min, almost 92% of cilostazol was released from CLZ-CD-MOFs, whereas only 26.3% of cilostazol was released for CLZ-I in 15 min. CLZ-I showed incomplete dissolution due to the poor solubility of cilostazol in water; in 90 min, only 63.3% of the drug was released. These findings demonstrate that under sink conditions, CD-MOFs effectively increase the dissolution of cilostazol.

Cytotoxicity study

MTT assay was used in cytotoxicity studies on human alveolar epithelial cells (A549). The CD-MOF possesses high porosity and surface area which promote internalization in cancer cell and induce cytotoxic effect such as apoptosis, necrosis of cancer cells due to generation of ROS [55]. Previous studies have reported the anti-inflammatory, antioxidant, and antiapoptotic actions of cilostazol [28, 30–32]. CLZ-CD-MOF-F3 demonstrated significant cytotoxic effects on A549 cells, with an IC50 value of 32.70 µg /ml. These results suggest CLZ-CD-MOF-F3 that hold promise as a potential compound against A549 cells.

Conclusion

DPI formulations of the poorly water-soluble drug cilostazol and porous metal–organic frameworks were efficiently formulated by vapor diffusion. The molecular modeling of cilostazol confirmed the nanocluster with CD-MOFs, i.e., its spatial molecular distribution and thermodynamic stability with free-energy estimation with or without CTAB. The synthesized CLZ-CD-MOFs possess an entrapment efficiency of approximately 96.39%, which was validated by the number of characterizations such as SEM, particle size distribution, flow property, PXRD, BET analysis, and molecular modeling, which include molecular docking and MD simulation. The CLZ-CD-MOFs showed cubic-shaped morphology with a large surface area and a consistent porosity structure. MOFs showed excellent in vitro pulmonary deposition with a large FPF value compared with commercial nonporous carriers and significantly improved cilostazol's solubility and dissolution. The cytotoxicity study on the A549 cell line showed the excellent cytocompatibility of CLZ-CD-MOF's. The γ-CD-MOFs offer enhanced solubility and aerodynamic performance for poorly water-soluble drugs, making them a promising pulmonary delivery approach.

Abbreviations

MOFs	Metal–organic frameworks
CD-MOF	Cyclodextrin metal–organic framework
DPIs	Dry powder inhalers
CTAB	Cetyltrimethylammonium bromide
MD Simulation	Molecular dynamics simulation
PDI	Polydispersity index
MMAD	Mean mass aerodynamic diameter
FPF	Fine particle fraction (FPF)
BRT	Brunauer–Emmett–Teller
CLZ-CD-MOF	Cilostazol–cyclodextrin metal–organic framework
SEM	Scanning electron microscopy

Acknowledgements

Not applicable.

Author contributions

P. Misar was involved in conceptualization, designing, material preparation, data collection and analysis K. Otari was involved in review and editing and supervision. P. Misar wrote the first draft of the manuscript. All the authors have read and approved the final version of the manuscript.

Funding

Not applicable.

Availability of data and material

Data will be made available on request.

Declarations

Ethics approval and consent to participate

Not applicable.

Consent for publication

Not applicable.

Competing interests

I declare that I have no financial and non-financial interests that may be relevant to submitted work including academic competition, intellectual property, or ideological beliefs. I confirm that there are no conflicts of interest regarding publication of this manuscript. If any potential conflicts arise during the review process or after publication, I will disclose them promptly to the editors.

Author details

[1]Dr. Babasaheb Ambedkar Technological University, Lonere, Raigad 402103, India. [2]N.N. Sattha College of Pharmacy, Ahmednagar 414003, India. [3]Navsahyadri Institute of Pharmacy, Nasrapur, Pune, Maharashtra 412213, India.

Received: 16 January 2025 Accepted: 18 August 2025
Published online: 26 August 2025

References

1. Liang D, Wang W, Chen G, Li J, Dou G, Gan H et al (2023) Cepharanthine dry powder inhaler for the treatment of acute lung injury. Molecules 28(11):4441

2. Hu X, Wang C, Wang L, Liu Z, Wu L, Zhang G et al (2019) Nanoporous CD-MOF particles with uniform and inhalable size for pulmonary delivery of budesonide. Int J Pharm 564:153–161
3. Zhou Y, Niu B, Wu B, Luo S, Fu J, Zhao Y et al (2020) A homogenous nanoporous pulmonary drug delivery system based on metal-organic frameworks with fine aerosolization performance and good compatibility. Acta Pharm Sin B 10(12):2404–2416
4. Li H, Zhu J, Wang C, Qin W, Hu X, Tong J et al (2020) Paeonol loaded cyclodextrin metal-organic framework particles for treatment of acute lung injury via inhalation. Int J Pharm 587:119649
5. Sun N, Zhang M, Zhu W, Song P, Dai T, Huang P et al (2023) Allyl isothiocyanate dry powder inhaler based on cyclodextrin-metal organic frameworks for pulmonary delivery. iScience 26(1):105910
6. Scherließ R, Bock S, Bungert N, Neustock A, Valentin L (2022) Particle engineering in dry powders for inhalation. Eur J Pharm Sci 172:106158
7. Zhou Y, Zhao Y, Niu B, Luo Q, Zhang Y, Quan G et al (2020) Cyclodextrin-based metal-organic frameworks for pulmonary delivery of curcumin with improved solubility and fine aerodynamic performance. Int J Pharm 588:119777
8. Huang Z, Lin L, McGoverin C, Liu H, Wang L, Zhou QT et al (2018) Dry powder inhaler formulations of poorly water-soluble itraconazole: a balance between in-vitro dissolution and in-vivo distribution is necessary. Int J Pharm 551(1–2):103–110
9. Lin L, Quan G, Peng T, Huang Z, Singh V, Lu M et al (2017) Development of fine solid-crystal suspension with enhanced solubility, stability, and aerosolization performance for dry powder inhalation. Int J Pharm 533(1):84–92
10. Liu T, Han M, Tian F, Cun D, Rantanen J, Yang M (2018) Budesonide nanocrystal-loaded hyaluronic acid microparticles for inhalation: in vitro and in vivo evaluation. Carbohydr Polym 181:1143–1152
11. Sawatdee S, Changsan N, Srichana T, Nanjwade B (2023) Porous particle technology: novel approaches to deep lung delivery. In: Pulmonary Drug Delivery Systems: Material and Technological Advances. Springer Nature Singapore, Singapore. p. 131–75.
12. Kumar M, Goswami P, Jha A et al (2024) Formulation and evaluation of cetuximab functionalized phospholipid modified nanocrystals of paclitaxel for non-small cell lung cancer therapy. Sci Rep 14:29114
13. Kumar M, Jha A, Bharti K, Manjit M, Kumbhar P, Dhapte-Pawar V et al (2024) Lipid-coated nanocrystals of paclitaxel as dry powder for inhalation: characterization, in-vitro performance, and pharmacokinetic assessment. Colloids Surf B Biointerf 237:113865
14. Zhou Y, Zhang M, Wang C, Ren X, Guo T, Cao Z et al (2021) Solidification of volatile D-limonene by cyclodextrin metal-organic framework for pulmonary delivery via dry powder inhalers: in vitro and in vivo evaluation. Int J Pharm 606:120825
15. Li X, Guo T, Lachmanski L, Manoli F, Menendez-Miranda M, Manet I et al (2017) Cyclodextrin-based metal-organic frameworks particles as efficient carriers for lansoprazole: study of morphology and chemical composition of individual particles. Int J Pharm 531(2):424–432
16. Xu Y, Rashwan AK, Osman AI, Abd El-Monaem EM, Elgarahy AM, Eltaweil AS et al (2023) Synthesis and potential applications of cyclodextrin-based metal–organic frameworks: a review. Environ Chem Lett 21(1):447–477
17. Al Sharabati M, Sabouni R, Husseini GA (2022) Biomedical applications of metal– organic frameworks for disease diagnosis and drug delivery: a review. Nanomaterials 12(2):277
18. He Y, Zhang W, Guo T, Zhang G, Qin W, Zhang L et al (2019) Drug nanoclusters formed in confined nano-cages of CD-MOF: dramatic enhancement of solubility and bioavailability of azilsartan. Acta Pharm Sin B 9(1):97–106
19. Xu J, Wu L, Guo T, Zhang G, Wang C, Li H et al (2019) A "Ship-in-a-Bottle" strategy to create folic acid nanoclusters inside the nanocages of γ-cyclodextrin metal-organic frameworks. Int J Pharm 556:89–96
20. Liu S, Xiong Y, Dong F (2024) Cyclodextrin metal–organic framework@ SiO2 nanocomposites for poorly soluble drug loading and release. RSC Adv 14(43):31868–31876. https://doi.org/10.1039/D4RA04935G
21. Huang Y, Tang H, Meng X, Liu D, Liu Y, Chen B et al (2024) Γ-cyclodextrin metal-organic frameworks as the promising carrier for pulmonary delivery of cyclosporine A. Biomed Pharmacother 171:116174
22. Neaz S, Alam MM, Imran AB (2024) Advancements in cyclodextrin-based controlled drug delivery: insights into pharmacokinetic and pharmacodynamic profiles. Heliyon. https://doi.org/10.1016/j.heliyon.2024.e39917
23. Bibi M, Ud Din F, Anwar Y, Alkenani NA, Zari AT, Mukhtiar M et al (2022) Cilostazol-loaded solid lipid nanoparticles: bioavailability and safety evaluation in an animal model. J Drug Deliv Sci Technol 74:103581
24. Pardhi VP, Patel P, Vaish A, Jain K (2024) Inclusion complexes of bedaquiline fumarate with β-cyclodextrin and its derivatives: in silico, in vitro and in vivo evaluation. J Drug Deliv Sci Technol 91:105253
25. Motta NA, Autran LJ, Brazao SC, de Oliveira LR, Scaramello CB, Lima GF et al (2021) Could cilostazol be beneficial in COVID-19 treatment? Thinking about phosphodiesterase-3 as a therapeutic target. Int Immunopharmacol 92:107336
26. Yang X, Xu Z, Hu S, Shen J (2023) Perspectives of PDE inhibitor on treating idiopathic pulmonary fibrosis. Front Pharmacol 14:1111393
27. Kabil SL (2018) Beneficial effects of cilostazol on liver injury induced by common bile duct ligation in rats: role of SIRT 1 signaling pathway. Clin Exp Pharmacol Physiol 45(12):1341–1350
28. Patel SG, Rajput SJ (2009) Enhancement of oral bioavailability of cilostazol by forming its inclusion complexes. AAPS PharmSciTech 10:660–669
29. Kherallah RY, Khawaja M, Olson M, Angiolillo D, Birnbaum Y (2022) Cilostazol: a review of basic mechanisms and clinical uses. Cardiovasc Drugs Ther. 1–6.
30. Li J, Xiang X, Gong X, Shi Y, Yang J, Xu Z (2017) Cilostazol protects mice against myocardium ischemic/reperfusion injury by activating a PPARγ/JAK2/STAT3 pathway. Biomed Pharmacother 94:995–1001
31. Hada Y, Uchida HA, Umebayashi R, Yoshida M, Wada J (2022) Cilostazol attenuates AngII-induced cardiac fibrosis in apoE deficient mice. Int J Mol Sci 23(16):9065
32. Groom CR, Bruno IJ, Lightfoot MP, Ward SC (2016) The Cambridge structural database. IUCrJ 3(2):171–179
33. Smaldone RA, Forgan RS, Furukawa H, Gassensmith JJ, Slawin AM, Yaghi OM et al (2010) Metal-organic frameworks from edible natural products. Angew Chem Int Ed Engl 49(46):8630–8634
34. Dallakyan S, Olson AJ (2015) Small-molecule library screening by docking with PyRx. In: Chemical biology: methods and protocols. p. 243–50.
35. Huey R, Morris GM, Olson AJ, Goodsell DS (2007) A semiempirical free energy force field with charge-based desolvation. J Comput Chem 28(6):1145–1152
36. Morris GM, Huey R, Lindstrom W, Sanner MF, Belew RK, Goodsell DS et al (2009) Autodock4 and Autodocktools4: automated docking with selective receptor flexibility. J Comput Chem 30(16):2785–2791
37. Bugnon M, Goullieux M, Röhrig UF, Perez MA, Daina A, Michielin O et al (2023) SwissParam 2023: a modern web-based tool for efficient small molecule parametrization. J Chem Inf Model 63(21):6469–6475
38. Meshram RJ, Bagul KT, Aouti SU, Shirsath AM, Duggal H, Gacche RN (2021) Modeling and simulation study to identify threonine synthase as possible drug target in *Leishmania major*. Mol Divers 25:1679–1700
39. Meshram RJ, Bagul KT, Pawnikar SP, Barage SH, Kolte BS, Gacche RN (2020) Known compounds and new lessons: structural and electronic basis of flavonoid-based bioactivities. J Biomol Struct Dyn 38(4):1168–1184
40. MacKerell AD Jr, Bashford D, Bellott ML, Dunbrack RL Jr, Evanseck JD, Field MJ et al (1998) All-atom empirical potential for molecular modeling and dynamics studies of proteins. J Phys Chem B 102(18):3586–3616
41. Mackerell AD Jr, Feig M, Brooks CL III (2004) Extending the treatment of backbone energetics in protein force fields: limitations of gas-phase quantum mechanics in reproducing protein conformational distributions in molecular dynamics simulations. J Comput Chem 25(11):1400–1415
42. Liu H, Hou T (2016) CaFE: a tool for binding affinity prediction using end-point free energy methods. Bioinformatics 32(14):2216–2218
43. Phillips JC, Braun R, Wang W, Gumbart J, Tajkhorshid E, Villa E et al (2005) Scalable molecular dynamics with NAMD. J Comput Chem 26(16):1781–1802
44. Jurrus E, Engel D, Star K, Monson K, Brandi J, Felberg LE et al (2018) Improvements to the APBS biomolecular solvation software suite. Protein Sci 27(1):112–128
45. Deshkar SS, Borde GR, Kale RN, Waghmare BA, Thomas AB (2017) Formulation of cilostazol spherical agglomerates by crystallo-co-agglomeration technique and optimization using design of experimentation. Int J Pharm Investig 7(4):164–171
46. Van Vleet MJ, Weng T, Li X, Schmidt JR (2018) In situ, time-resolved, and mechanistic studies of metal–organic framework nucleation and growth. Chem Rev 118(7):3681–3721

47. Satari N, Taymouri S, Varshosaz J, Rostami M, Mirian M (2020) Preparation, and evaluation of inhalable dry powder containing glucosamine-conjugated gefitinib SLNs for lung cancer therapy. Drug Dev Ind Pharm 46(8):1265–1277
48. Liu B, Li H, Xu X, Li X, Lv N, Singh V et al (2016) Optimized synthesis and crystalline stability of γ-cyclodextrin metal-organic frameworks for drug adsorption. Int J Pharm 514(1):212–219
49. Gawali VU, Patil PB, Chede SM, Jagdale SC, Kuchekar BS, Chabukswar AR (2009) Studies on cilostazol and β-cyclodextrin inclusion complexes. Int J Pharm Bio Sci 1(4):1073–1078
50. Kadota K, Yanagawa Y, Tachikawa T, Deki Y, Uchiyama H, Shirakawa Y et al (2019) Development of porous particles using dextran as an excipient for enhanced deep lung delivery of rifampicin. Int J Pharm 555:280–290
51. Chvatal A, Ambrus R, Party P, Katona G, Jójárt-Laczkovich O, Szabó-Révész P et al (2019) Formulation, and comparison of spray dried non-porous and large porous particles containing meloxicam for pulmonary drug delivery. Int J Pharm 559:68–75
52. Borah C, Saikia T, Bharali A, Lahan M, Biswas N, Sahu BP (2024) Development of Paclitaxel proliposomal dry powder inhaler (PTX-PLM-DPI) by freeze-drying method for lung cancer. Drugs Drug Candidates 3(1):275–290
53. Fronius M, Clauss WG, Althaus M (2012) Why do we have to move fluid to be able to breathe? Front Physiol 3:146
54. Velaga SP, Djuris J, Cvijic S, Rozou S, Russo P, Colombo G et al (2018) Dry powder inhalers: an overview of the in vitro dissolution methodologies and their correlation with the biopharmaceutical aspects of the drug products. Eur J Pharm Sci 113:18–28
55. Kumar M, Goswami P, Jha A, Dhapte-Pawar V, Koch B, Mishra B (2025) Formulation and evaluation of lipid/Soluplus-stabilized nanocrystals of Paclitaxel and Bosutinib for a synergistic effect in non-small cell lung cancer therapy. Mol Pharm. https://doi.org/10.1021/acs.molpharmaceut.4c01334

Publisher's Note